Optimal alignment of coastal bathymetry data using fast normalized cross-correlation

Abstract

Statistical analysis of beach profile data collected from a laser elevation scanner in a series of experiments at the Queen's University Coastal Engineering Laboratory is presented. The dataset consists of beach profile measurements under wave conditions when reinforced with coir fiber, a waste material from coconut production. A three-step alignment process was used to correct the profile elevation data, consisting of global, mid-level, and local adjustments. The global alignment process designated a consistent zero for all profiles, and was used to correct major discontinuities. The mid-level alignment process was applied to average the final 25% of the previous scan with the first 25% of the following scan, and apply offset values to the following scan. The local alignment used a two-dimensional fast normalized cross-correlation method to find the optimal offset in both the horizontal and vertical directions, and was used to find the best match with overlapping adjacent bathymetry scans. Collectively, the three scales of adjustment provide a computationally fast method to align continuous data along a consistent profile, and can potentially be applied to topographic and bathymetric observations collected during storm events.

My signature below attests that this submission is my original work

Following professional engineering practice, I bear the burden of proof for original work. I have read the Policy on Academic Integrity posted on the Civil Engineering departmental web site (www.civil.queensu.ca/undergraduate) and confirm that this work is in accordance with the Policy.

Signature: _____ Date: _____

Table of Contents

Index of Figures

Index of Tables

Index of Equations

1   Introduction

Protecting coastlines from erosion and flooding is a continuous problem for coastal communities, a challenge now amplified due to projected sea-level rise and increased storm intensity (Berard et al., 2016). This problem has been addressed in a variety of ways, one of which focuses on the protection of sand dunes using reinforcing materials that include hard structures (rock, concrete), soft structures (sand), or bio-engineered materials (vegetation). Coir (coconut) fibre is a bio-material derived from coconut production that is currently being investigated for use as an economical and environmentally sustainable shore protection.

A series of experiments were completed by N. Mathura in 2012 to study the response to sand dunes under a variety of two-dimensional wave conditions. These experiments were conducted in the wave basin at the Coastal Engineering Lab at Queen's University, and measurements of the waves and morphology changes were collected. Tests were run for the sand beach profile with and without a coir fibre bio-log.

The present research investigates the bathymetic survey results from these tests using alignment techniques on three different spatial scales, including a 2-dimensional cross-correlation to adjust the vertical and horizontal positions of adjacent surveys to maximize the cross-correlation coefficient. This statistical method of cross-correlational is used in image matching applications (Lewis, 1995), and its application to beach profile data alignment in the present study is novel. The three step process used has a variety of potential applications to correct discontinuities introduced during data collection.

1.1   Background

Around the world, coastlines experience morphology changes due to a variety of geophysical factors. These include the forces introduced by the processes of waves, water level changes, wind, runoff, groundwater, and currents, all of which deliver energy, induce sediment transport and reshape the shore (Lindsay, et al., 1992; O'Connell, 2002) . Periodically coastlines are exposed to major weather events such as hurricanes, which create more powerful waves and cause more severe damage in combination with higher water levels. These storms can cause sudden and severe erosion, resulting in flooding that endangers property and life (Beylard, et al., 2015).

The intensity of storm surge and waves could increase in the future due to climate change, since rising sea-levels increase risks of property damage and higher storm intensity increases coastal hazards (Beylard, et al., 2015). Notably, Hurricane Katrina in 2005 caused 1830 fatalities and $108 billion USD ($131 billion in 2015 dollars), largely due to its 10 m storm surge (Berard, et al., 2016). Climate change has the potential to significantly increase the risk to coastal environments in the future.

Development and population growth along coastlines is advancing at a rapid rate. For example, Australian coastal communities are growing 60% faster than inland ones (Hornsey, et al., 2011), a trend also occurring in North America (O'Connell, 2002). Protecting growing communities from destructive coastal processes has become a complex and growing challenge. Many existing techniques for shoreline protection have drawbacks, including regulatory hurdles (including property rights), environmental issues, aesthetic challenges, poor performance, and low willingness of governments to fund improvements for coastal protection (Lindsay, et al., 1992; O'Connell, 2002).

1.2   Literature Review

This literature review focuses on physical models of beaches that have been built to investigate beach reinforcement techniques, the properties of coir fibres, and the cross-correlation method used for alignment.

1.2.1   Physical Modeling

Physical experiments have been completed to model changing dune shape under coastal conditions. These experiments are usually done to either directly gain an understanding of coastal processes on dunes, or to validate numerical models. By conducting erosion tests of dunes under storm conditions, their performance as coastal defences can be evaluated and quantified (Beylard, et al., 2015). Laboratory experiments typically consist of a wave flume with a beach profile, instrumented with wave and water depth gauges at regular intervals. The results from the change in depth and dune profile then provide a view of the impact from erosion.

A widely-cited early experiment of beach profile erosion was the *Delta Flume '93 Experiment.* This experiment subjected a beach profile and dune to waves in a 225m long and 5m deep flume. The experiment subjected the beach morphology to different wave conditions, but did not model overwash or inundation conditions (Arcilla, et al., 1994).

Recent studies categorize storms using the *Storm Impact Scale.* This scale divides storms into four regimes: Swash, Collision, Overwash, and Inundation; with each categorizing a progressively stronger storm. The swash and collision regimes represent water levels below the base of the dune and at the base of the dune, respectively. The overwash regime is defined by where the wave height occasionally reaches the upper limit of the dune. Finally, the inundation regime is a storm where the water level is above the top of the dune, flooding the area inland (Sallenger, 2000).

Tests by Tomasicchio et al. (2011) were conducted in a 100 m long and 5 m deep flume to calibrate the C-SHORE numerical model for the collision regimes at two different water levels. The experiment was not conducted in the inundation regime, and did not attempt to simulate a dune with reinforcements.

Recent studies conducted at Queen's University modeled dunes in a wave flume (35.5 m long and 1.2 m deep). These experiments, conducted by Berard et al. (2016) and Beylard et al. (2015), verified the results of the XBeach numerical model and modeled the reactions of dunes to the inundation regime respectfully. The results from the inundation regime test were found to be significantly different than the overwash regime, with the dune erosion occurring at a much faster rate.

1.2.2   Beach Reinforcement and Biomaterials

A wide variety of materials such as rock, concrete, sand, or biomaterials are currently in use to prevent beach and dune erosion. These materials function either by providing reinforcement to the sand or by adding an additional layer of protection on top of the dune. Traditional rigid materials like rock or concrete provide structural strength, such as seawalls, revetments, and bulkheads. Although considered to be effective, these structural solutions are declining in popularity, due to environmental, atheistic, and regulatory concerns (Kraus, 1998; O'Connell, 2002).

As an alternative, numerous types of biomaterials are currently being investigated. These include vegetation to reinforce sand, or manufactured products such as geomembranes, cotton netting, and bio-logs or bio-tubes. These depend on site-specific conditions, but show considerable promise for shore protection applications (O'Connell, 2002).

One technique is the use of vegetation, either through the form of coastal wetlands or dune reinforcement. Although there is disagreement about the impacts that vegetative protection has, the majority of evidence suggests that it is an effective way to mitigate flooding and erosion risks (Gedan, et al., 2011). One case study is of a beach in Massachusetts suffering from significant erosion due to frequent storms. To combat this, dunes with a "z-pattern" of beach grass were installed to increase the stability of the dunes during overtopping events, while maintaining the ecology of the area. One notable complication of this method is the possible requirement for nitrogen fertilizer, which can create runoff issues if not managed effectively (O'Connell, 2002).

Geotextiles and geomembranes have also been investigated and have significant potential for beach protection. In particular, geotextile sand containers (GSC) are geotextile tubes or bags filled with sand, either as a smaller individual container (less than 2.5m^3) or as a larger tube (greater than 2.5m^3). These containers are presently available in a variety of sizes, fill materials, and fabrics. Both laboratory and field testing has been completed on GSC structures, with promising results. GSCs were identified to remain stable in wave conditions with slopes up to 1:2, and have exhibited failure rates below 10-15% in field testing (Hornsey, et al., 2011). GSC structures are also relatively simple to install and maintain, and show the ability to withstand the loss of a small number of containers. However, the relatively thin exterior is vulnerable to cutting by sharp objects, making vandalism and accidental or environmental damage a major issue. While this is somewhat mitigated by the independent nature of GSCs, it remains a drawback to this method (Restall, et al., 2002).

1.2.3   Coir Fibres

Coir fibres are fibres derived from coconut production and are a biomaterial currently receiving significant research focus. These fibers are traditionally collected by soaking coconut husks in ponds or lagoons, and recently enzyme solutions have been used to speed up the process from months to days. Presently, this fibre is used to create ropes, geotextiles, and composites, but is often treated as waste material and disposed of. Of the 512 thousand tons of coconut fibre produced annually around the world, only a small percentage is recycled (Mathura, et al., 2015).

On a small scale, testing of coir fibers has determined the tensile strength to be 78 to 118 MPa, with higher strength when soaked in salt water (Mathura, 2012). Recent tests at Queen's University measured a slightly higher range of 139 to 100 MPa, with variations due to retting time and materials (Mathura, et al., 2015). Furthermore, tests revealed that the fibres lost approximately 30% of their overall strength after 2 years of wetting and drying, with minimal swelling of 5% (Mathura, 2012). These results are promising for geotextile use with the fibers being sufficiently strong and durable to withstand coastal conditions.

Coir fibres have several non-structural properties that support their usage for coastal stabilization in some tropical locations. For example, they are readily available in the Caribbean region. The fibres are environmentally stable, with bio-logs easily conforming to the shape of the beach surface, and degrading into organic material. The material also has the potential to create other economic benefits by improving the shoreline while recycling a locally produced waste material (Mathura, 2012).

In India, a pilot-scale test was conducted on an eroding river using a coir fibre mesh to protect a bank slope while vegetation was given time to grow. This test was largely successful, with growth outside the geotextile reinforced area being approximately 1/3rd of the vegetative growth within the reinforced section. The experiment also noted the relative simplicity in the construction of this project, as well as the low cost (Joseph & Sarma, 1995).

1.2.4   Cross-correlation

A normalized two dimensional cross-correlation technique was used to match the beginning section of one profile with the end segment of the proceeding profile. This is a novel application of cross-correlation that has not been used in this way before; however, the underlying theory has been applied in computer vision applications to track specific items (or templates) as they move across a scene on time.

Cross-correlation attempts to quantify the similarity between two datasets, and can be applied in two dimensions to understand this similarity as a function of both x and y. Cross-correlation can be described as (Lewis, 1995; Haralick & Shapiro, 1991):

$$c(u,v) = \sum_{x,y} f(x,y)t(x-u, y-v)$$

Equation 1: Cross-correlation function

Where c is the correlation coefficient at all points in a matrix, f(x,y) is the original matrix being evaluated against (with x and y being matrix points), and t is the matrix being evaluated (with u and v as matrix points). Lewis then expanded this technique into the normalised form that was used for this analysis, eliminating the impact that variations in intensity and edges caused.

$$\gamma(u,v) = \frac{\sum_{x,y}\left[f(x,y) - \bar{f}_{u,v}\right]\left[t(x-u, y-v) - \bar{t}\right]}{\left(\sum_{x,y}\left[f(x,y) - \bar{f}_{u,v}\right]^2 \ \sum_{x,y}\left[t(x-u, y-v) - \bar{t}\right]^2\right)^{0.5}}$$

Equation 2: Normalized 2D cross-correlation function

Where f is the section of the previous profile (with x and y being matrix points), $\bar{t}$ is the mean of the profile being matched, and $\bar{f}_{u,v}$ is the mean of the f(x,y) region overlapped by the matched profile (with u and v as matrix points). The matrix form of the function is implemented in MATLAB 2015b as the *normxcorr2* function.

1.3   Objective

The original goal of this study was to examine the impact of the coir fiber on the beach profile, and to compare these values to existing literature. However, inconsistencies in the dataset limited this analysis and a new goal was defined to develop a method for automatic numerical alignment of overlapping bathymetry scans.

2   Experimental Setup

The experiment that was conducted under conditions identical to those used by (Berard, et al., 2016). The experiments were conducted in a 22.75 m long by 0.70 m deep wave flume inside a rectangular wave basin using a piston-type wave paddle. The paddle was computer controlled and generated an irregular wave pattern following a JONSWAP spectrum with a significant wave height of 0.16m and a peak period of 2.13s. The paddle was not equipped with reflection compensation, possibly creating a source of error within the dataset. This basin was instrumented with eight capacitance-type water level probes sampling the water level to a resolution of 0.1 mm at a frequency of 20 Hz located along the flume centreline.

The beach profile was created using silica sand with a D_{50} of 0.165 mm. The profile then had a thin layer of slightly larger sand mixed with Portland cement layered on top to preserve the granular roughness. The profile was measured using a laser profiler with horizontal and vertical resolutions of 0.0016 m and 0.4 μm respectively.

The wave height and beach morphology were measured continuously as the test progressed. The test was run at different wave conditions, and both with and without the coir fibres as protection. These results will be analyzed during this investigation.

3   Analysis Methodology

A series of adjustments were performed on the collected scan profiles in order to align the results along a single cohesive curve, matching the bed form that was visible in the experimental result. Scans were collected in 100 mm sections, with approximately 50 mm of overlap. The number of scans collected for a profile varied, but was always less than 94 files. Since each scan covered an additional 50 mm, the total distance collected never exceeded 4700 mm along the flume. All processing was done using MATLAB 2015a. For the purposes of this alignment, the x-axis was taken to be the length along the flume, while the z-axis was the vertical measure of the profile.

3.1   Data import and global alignment

Scans were imported following a bath process based on file names using the MATLAB *xlsread* function. Gaps in the profile without any recorded data were skipped, and all available x and z-values were saved based on the scan's reported start point. In rare cases of duplicate z values for a single x-coordinate, the z-values were averaged to produce a single result.

Without any processing there were a number of inconsistencies in the dataset (Figure 1). Individual profiles did not start at a consistent height, and had significant jumps where the laser profiler was moved closer to the bed. Furthermore, there were large gaps between individual scans within the profile.
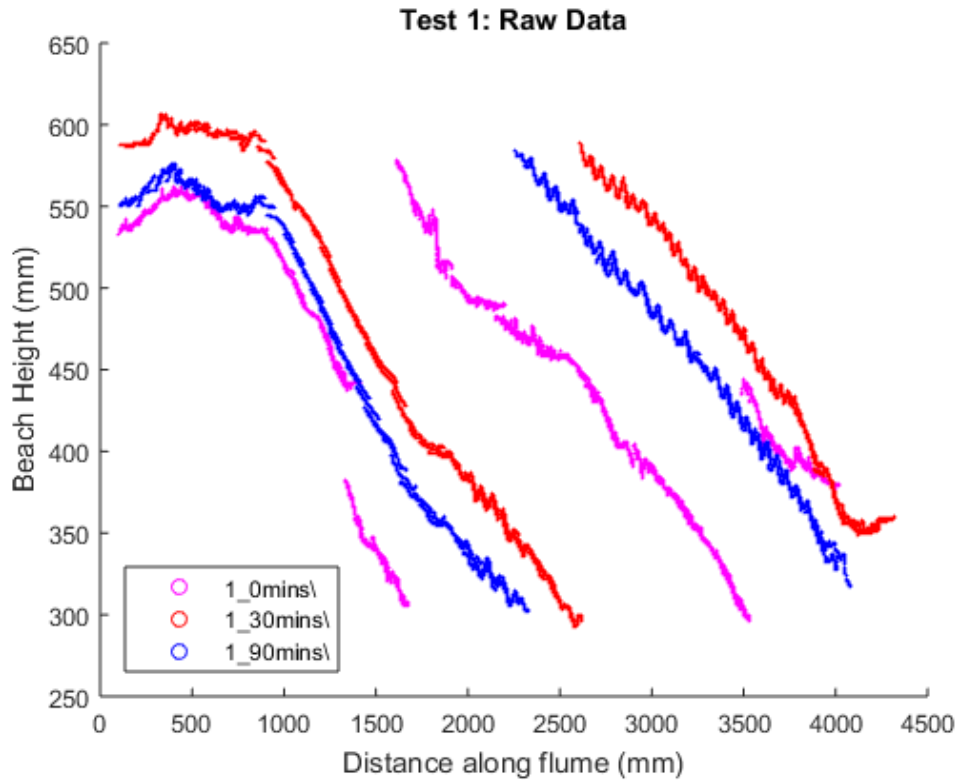
Figure 1: Raw data imported from scans

The first attempt at alignment corrected these large discontinuities by defining them as two consecutive scans with a vertical change of more than 150 mm. In these cases, the start point of the farther scan was set as equal to the endpoint of the proceeding scan. Furthermore, the starting points of all profiles were set to the same start point as the first profile for a given test. For both of these alignments, the adjustment was carried out on all subsequent scans in a profile (Figure 4).

3.2   Mid-level alignment

A second alignment was then applied in order to further improve the smaller discontinuities between scans. This method was implemented by averaging the final quarter of the proceeding scan, and then adjusting the values of the following scan so that the first quarter had the same average value (Equation 1):

$$\Delta z_t = \frac{\sum_{n=3*(\frac{N_{t-1}}{4})}^{N_{t-1}} z_{n,t-1}}{\frac{N_{t-1}}{4}} - \frac{\sum_{n=1}^{\frac{N_t}{4}} z_{n,t}}{\frac{N_t}{4}}$$

Equation 3: Mid-level alignment function

Where Δz_t is the offset for a given scan, n_t is a particular x,z point within a scan, N_t is the total number of points within a given scan, $Z_{n,t}$ is the z coordinate for a given scan at a given point.

This offset was then applied to all points in a scan, as well as all subsequent scans (Figure 5, Figure 6).

3.3   Local alignment

A final alignment using a normalized two-dimensional cross-correlation was then performed in order to further refine correlations between overlapping scans. This was implemented by looking at the first 85 points (representing approximately 15 mm) of the scan to be aligned and 110 points of the preceding scan (approximately 20 mm). This protocol allowed for 5 mm of adjustment to be applied in both the vertical and horizontal directions. The readings from the laser scanner were then rounded to the nearest 0.1 mm to simplify the alignment process by interpolating all points on a 2D binary grid.

The *normxcorr2* function in MATLAB 2015a was applied in order to find the cross-correlation using the method described in Equation 2. This function produced a matrix showing the correlation coefficient at all points, with lags applied in both the x and z-axis. The result of this operation can be visualized using the *pcolor* function (Figure 2).
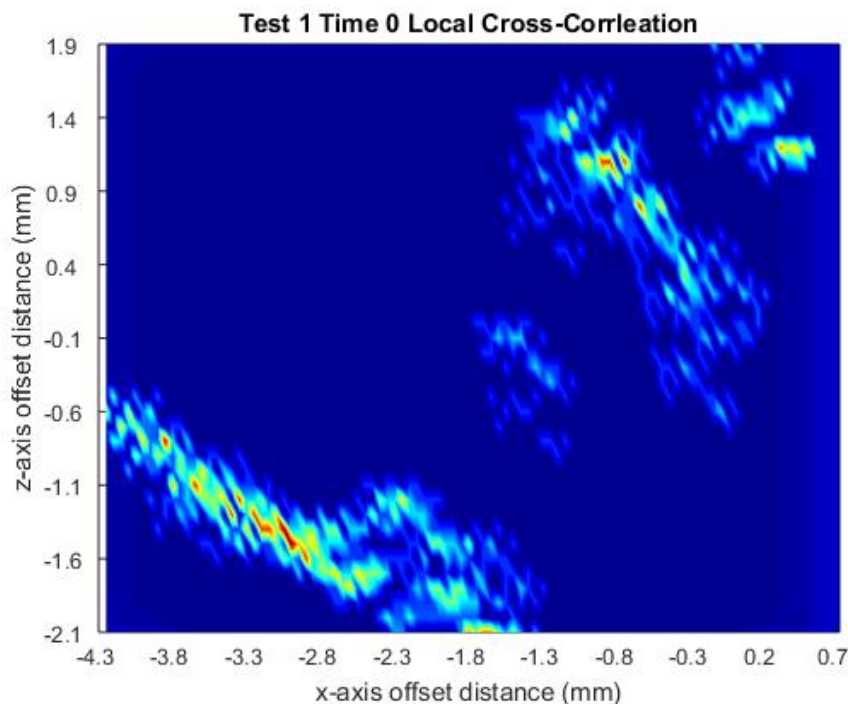
Figure 2: Heat map of plot of correlation coefficients for different alignments

This matrix was then smoothed using a Gaussian filter, which adjusts the values according to the surrounding points. This is defined as:

$$g(x, z) = \frac{1}{2\,\pi\,\sigma^2} * e^{-\frac{x^2 + z^2}{2\,\sigma^2}}$$

Equation 4: Gaussian filter

Where x and z are their respective axis and σ is the standard deviation on the distribution. For this analysis, the *imgaussfilt* function was applied with a standard distribution of 2. As an additional parameter, the nearest 5 points were evaluated, smaller than the default value of 9, to prevent oversmoothing. This filtered matrix was visualized using *pcolor* (Figure 3).
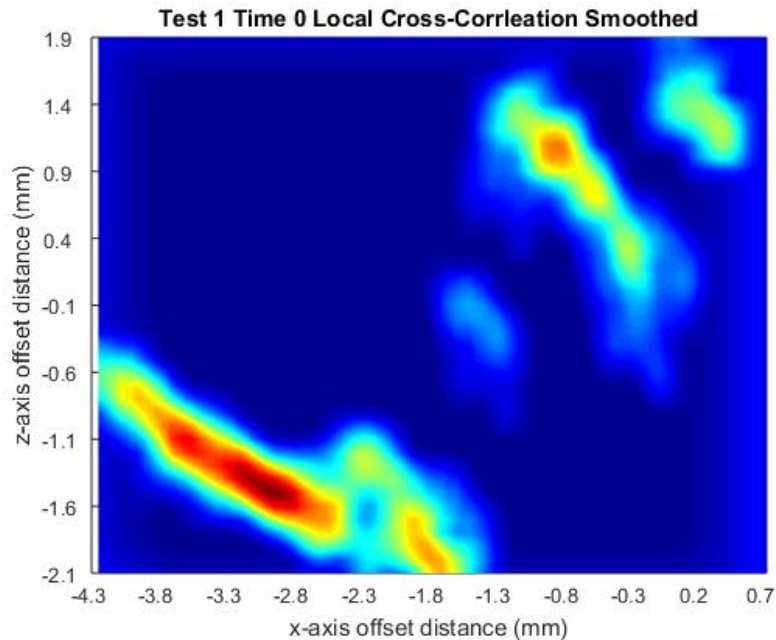
Figure 3: Heat map (Figure 2) smoothed with Gaussian filter

The maximum point in the smoothed matrix was taken as the offset (approximately -3 mm in the x-axis, and -1.5 mm in the z-axis), and applied to every point in the scan being investigated. The cumulative sum of all offsets was applied to each subsequent scan to provide continuity throughout the profile.

4   Results

Although the alignment process significantly improved the profiles as seen in Appendix A, no results were drawn from the impacts of the coir fibers. A variety of factors contributed to this, including the remaining uncertainty arising from the slight discontinuities in the alignment, as well gaps in the information on the experimental conditions for each test. However, an analysis on the effectiveness for each alignment methodology was completed.

4.1   Global Alignment

The global alignment produced the most dramatic improvement to the profile. By broadly eliminating large gaps between scans, the overall shape of the measured profile became much more visible. The end to end offset correctly adjusted these jumps on a macro scale due to the overlap between scans, but did not make any smaller order improvements. Adjusting the starting point to be even for all tests again showed a dramatic improvement by allowing the shape to be better compared through time, in particular the critical first section of the bed.

Significant local discontinuities remained after this process was completed. Jumps that did not meet the 150 mm threshold for a sensor movement correction but were still large were not corrected (Figure 4).
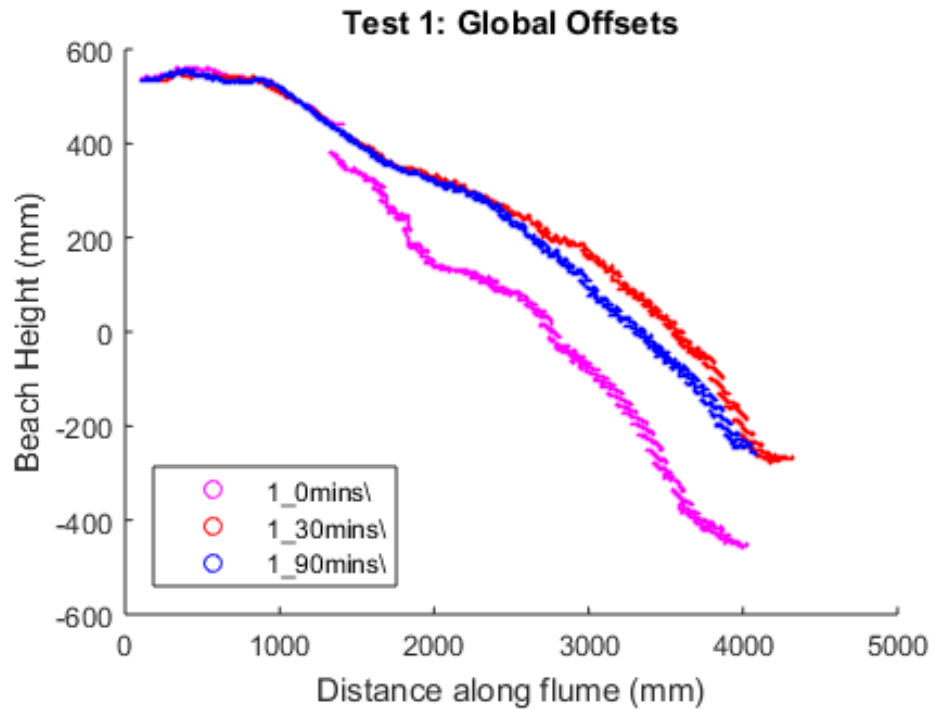
Figure 4, Beach profile for test 1, global correction applied

4.2   Mid-level Alignment

The mid-level alignment was much more successful at correcting local discontinuities, and significantly improved the continuity of the overall profile. Figure 5 plots the mid-level alignment profile against the globally aligned profile, and shows several of the improvements that resulted from this technique. In particular, scans at the end of the bar were much better aligned, and drops in the mid-section of the profile were successfully corrected.
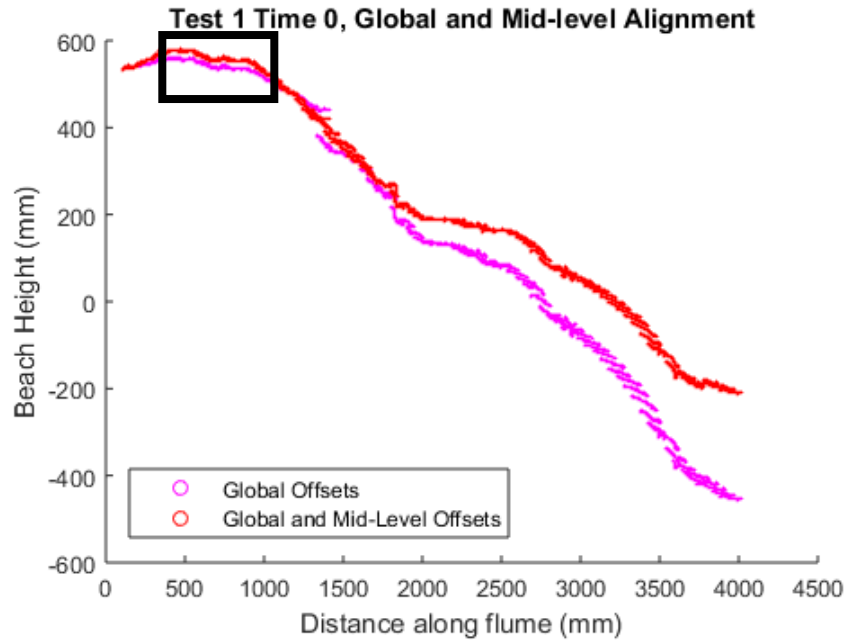
Figure 5: Test 1 time 0 profile with global and mid-level alignment

This technique had a major downside of introducing additional discontinuities in some parts of the bar. Since the first and last quarter of each scan was aligned, scans with significant overlapping (often in the steeper sections of the profile) were incorrectly offset, and were aligned lower than the previous scan (Figure 6). However, on an overall basis this technique demonstrated considerable from the global alignment alone.
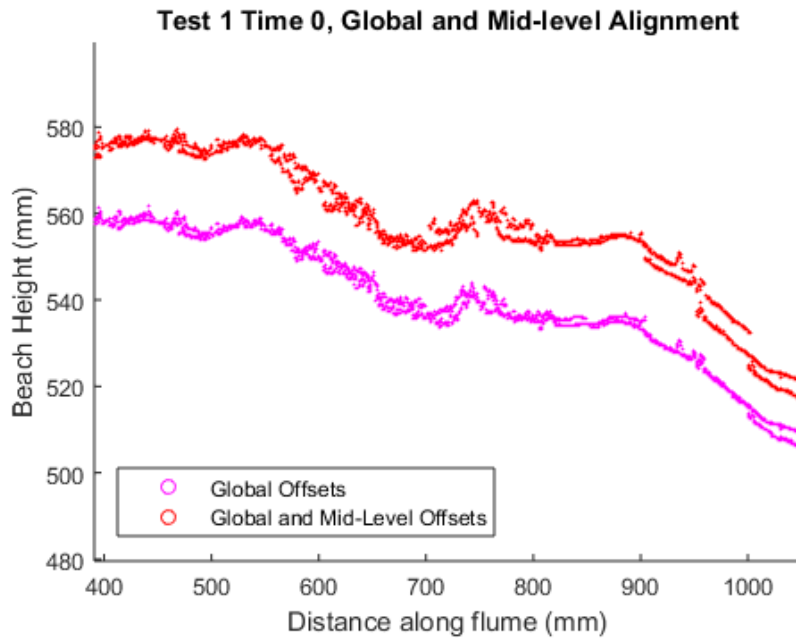
Figure 6: Zoom of Figure 5 region of interest

4.3   Local Alignment

The cross-correlation method applied in the local alignment further improved the continuity of the profile. By allowing for scans to be slightly adjusted horizontally, corrections from recorded horizontal values could be automatically applied to each scan. Although this correction had limited effect on the overall length, individual scans were better aligned throughout the bed. The overall profile follows the shape of the mid-level alignment with some minor differences throughout the bed (Figure 7).
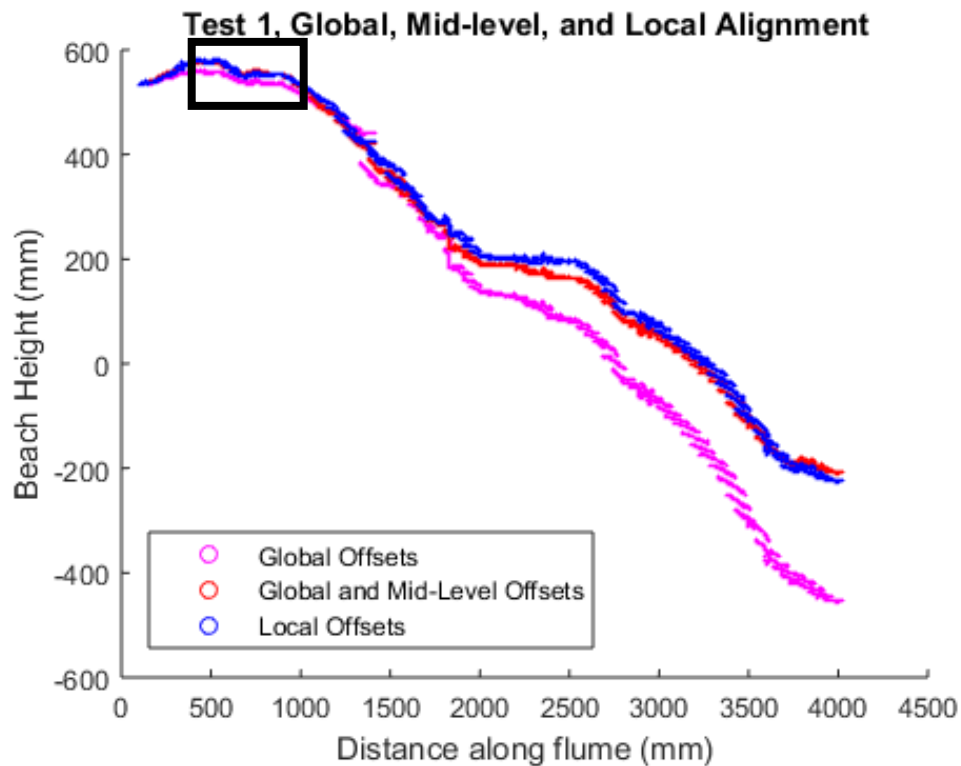
Figure 7: Test 1 time 0 with global, mid-level, and local offsets

Figure 8 shows the impact of matching based on the shape of the profile as opposed to a simple average value. Complex scans have improved alignment, while most of the discontinuity in the more linear sections introduced by the mid-level alignment is corrected (as seen on the far right of the figure). However, some discontinuities remain visible, which this methodology was unable to correct.
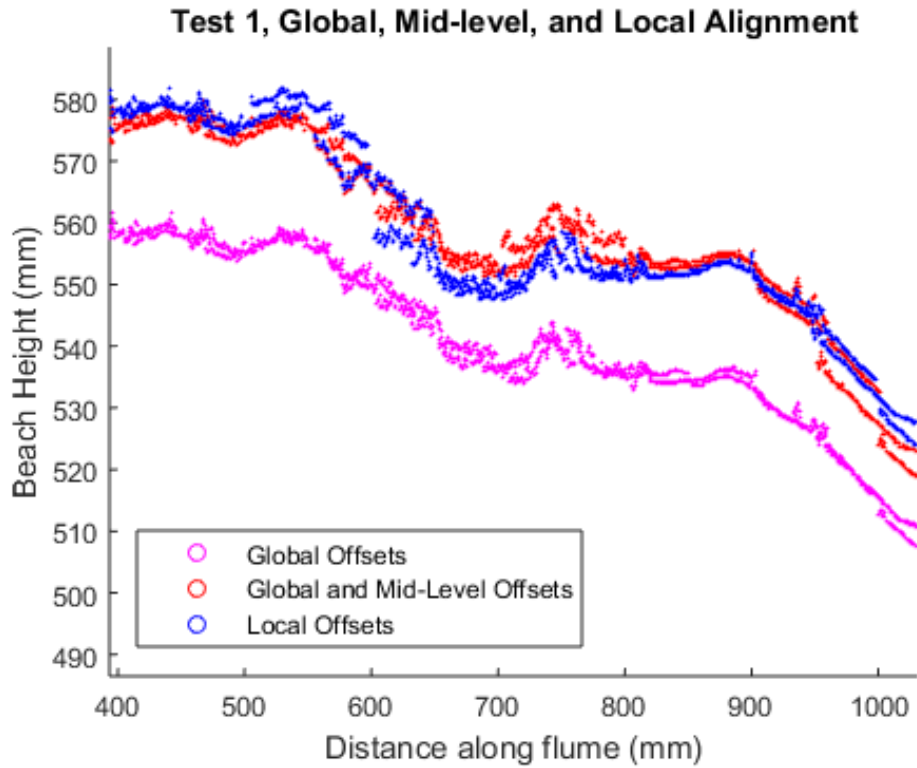
Figure 8: Zoom of Figure 7 area of interest

4.4   Quantitative Results

In order to quantify the effectiveness of the selected alignment methodologies, the difference between the last quarter of a scan and the first quarter of the following scan were compared across tests (Equation 3). Although this method did not capture the entire alignment quality, it provided a broad overview of the success of each method.

Table 1 shows the result of this process averaged over all tests. As expected, the mid-level alignment provided the best result. Since the measurement process is identical to the evaluation method, and the local horizontal offset complicates the process. Notably, both methods demonstrated considerable improvement relative to global alignment alone.

Table 1: Averaged differences for entire profile

Global Only	Global + Mid-level	Global + Mid-level + Local
7.06	0.01	2.07

Since the key area of interest for the evaluation was the initial sections of the bed, a second comparison was created showing the difference in only the first 40 points of the bed (Table 2). This comparison more accurately reflected the alignment in the key area of interest.

Table 2: Averaged differences for first 40 points in profile

Global Only	Global + Mid-level	Global + Mid-level + Local
4.93	0.0858	1.69

The smoothed R-value along the length of the profile for Test 1 Time 0 was also recorded for every test, with results from Test 1 Time 0 plotted in Figure 9. There was no significant trend in the correlation coefficient along the bed; however, the variation in R-value is visible. Critically, several alignments where no possible cross-correlation was found are visible with an R-value of zero. In these cases, no local alignment was performed.
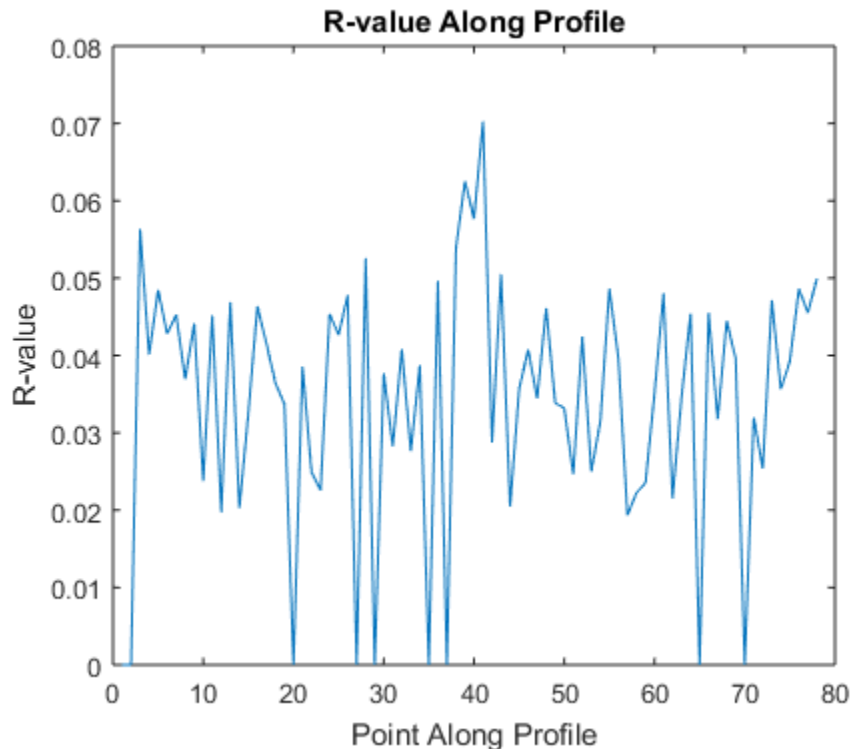
Figure 9: Smoothed R-value along profile Test 1 Time 0

4.5   Overall Effectiveness

As shown in Appendix A, the local alignment method was applied to all collected data, comprising of variations on 5 conditions with a total of 8 tests. Within each test, about four time points were recorded, for a total of 43 separate profiles ().

Overall, the process was effective at aligning most profiles along a continuous curve. Although there are still uncertainties in the results arising from the correction, the profiles represent a realistic set of experimental data. Specifically, test 2N provides a good indicator of the expected profile for this style of test, with a profile eroding at the upper sections through time under wave action. This is in contrast to several of the tests where the profile appears to gain height through time, indicating problems in the data.

5   Discussion

Although specific improvements were difficult to quantify, qualitatively the alignment improved with each degree of subsequent alignment applied, resulting in an overall process that was capable of

determining an overall profile from discontinuous scans. The global alignment was necessary for finer grained processing to be applied to the data, and allowed for a quick and straightforward comparison of trends.

The mid-level alignment acted as an initial guess for close alignment between scans. Although in some cases it resulted in greater discontinuities, the process reduced the discontinuity between scans overall. Importantly, this method was able to correct medium sized jumps between scans, which was required for the local alignment.

The local alignment process represented a novel application of the 2-dimentional normalized cross-correlation function built into MATLAB. This method was pioneered for use in computer vision and object tracking, and its application to scan registration was largely successful in improving the alignment for small differences in scans.

As profiled in Table 1 and Table 2, alignments improved in varying degree for different sections of the bar. The results match the trends visible in the profile plots, with the global alignment improving in this section relative to the entire bed along with the local alignment. The local alignment's effectiveness in complex areas is a likely source of this improvement in the area, as there was significantly more variability in the scans. This result is particularly notable due to the higher significance of the results near the top portion of the dune when investigating the impact of coir fiber.

Collectively, the alignment process improved the ability to see the overall trend in the profiles. Although interpretation is limited due to other gaps in the data, the methodology was successful in improving the collected data.

5.1   Potential Applications

By providing a computationally fast process for determining alignment in two directions, this method has a number of potential applications beyond the case studied here. In particular, to this area of study it could be applied to sequential scans taken in poor conditions. This method requires confidence in each individual scan, sufficient overlap between scans, and a known zero point. When these conditions are present (for example, during aerial observations or during storms), scans can be successful aligned into a cohesive profile to identify changes through time. The second and third steps in particular have considerable potential to be applied in series to increase the accuracy of the overall results.

Beyond coastal engineering, this application has unique merit through the fast speed of alignment. Potential signal processing applications center on cases where there are a large number of data points that require alignment, and in particular cases where a sufficiently complex signal to improve the cross-correlation process is available.

6   Conclusion

Experiments were completed at Queen's University to study the impact coir fibre would have on coastal erosion under wave conditions. Data from the tests included a series of 10 cm bathymetry elevation scans using a laser profiler, with overlap between scans. Upon analysis, there were a significant number of discontinuities between scans, making interpretation of the overall profile impossible.

A three-step alignment process was developed to correct the profile elevation data, with each level refining the previous method. A global offset successfully corrected large jumps in the scans where the

laser profiler was moved, as well as equating the starting points of all profiles. This was further enhanced by a mid-level offset, which brought local scans closer to a consistent alignment. Finally, the use of a fast normalized two-dimensional cross-correlation determined offsets in both the vertical and horizontal axis, allowing for a more localised adjustment.

This process has the potential to be applied to a number of applications. Notably, alignment may be useful in cases when precise control on data cannot be ensured, such as during severe storm events. The computationally efficient nature of this process also allows for rapid application to large datasets using minimal computing resources.

7   Acknowledgements

8   References

Arcilla, A. et al., 1994. The Delta Flume '93 Experiment. In: *Coastal Dynamics '94: Proceedings of an International Conference on the Role of the Large Scale Experiment in Coastal Research.* Barcelona, Spain: Universitat Oiktecnica de Catalunya, pp. 488-502.

Berard, N., Mulligan, R., da Silva, A. & Dibajnia, M., 2016. Morphological Evolution of a Sand Dune Exposed to High Water Levels and Bichromatic Wave Forcing. *Coastal Engineering.*

Beylard, B., da Silva, A. & Mulligan, R., 2015. *A Laboratory Investigation of Wave-Driven Dune and Beach Morphology Change Under High Storm Surges.* The Hague, Netherlands, s.n.

Gedan, K. et al., 2011. The present and future role of coastal wetland. *Climate Change,* 106(1), pp. 7-29.

Haralick, R. M. & Shapiro, L. G., 1991. *Computer and Robot Vision.* 1st ed. Boston: Addison-Wesley.

Hornsey, W., Carley, J., Coghlan, I. & Cox, R., 2011. Geotextile Sand Container Shoreline Protection Systems: Design and Application. *Geotextiles and Geomembrances,* 29(4), pp. 425-439.

Joseph, G. & Sarma, U., 1995. *Retted (White) Coir Fiber Netting- The Ideal Choice as Geotextiles for Soil Erosion Control,* Kerala, India: Coir Research Institute.

Kraus, N., 1998. The Effects of Seawalls on the Beach: An Extended Literature Review. *Journal of Coastal Research,* Special Issue(4), pp. 1-28.

Landry, B., Hancock, M., Mei, C. & Garcia, M., 2012. WaveAR: A software tool for calculating parameters for water waves with incident and reflected components. *Computers & Geosciences,* Volume 46, pp. 34-43.

Lewis, J. P., 1995. *Fast Normalized Cross-Corrleation,* San Francisco: Industrial Light & Magic.

Lindsay, B., Halstead, J., Tupper, H. & Vaske, J., 1992. Factors Influencing the Willingness to Pay for Coastal Beach Protection. *Coastal Management,* Volume 20, pp. 291-302.

Mathura, N., 2012. *Sustainable Coastal Engineering in the Caribbean: A Coir Fiber Approach,* St. Augustine: ICE Young Professionals and Students Paper Competition.

Mathura, N., Cree, D. & Mulligan, R., 2015. *Characterization and Utilization of Coconut Fibers of the Caribbean,* Kingston, Ontario: Queen's Univeristy.

O'Connell, J., 2002. *Stabilizing Dunes and Coastal Banks using Vegetation and Bioengineering: Proceedings of a Workshop held at the Woods Hole Oceanograpghic Institution.* Woods Hole, MA 02543, Woods Hole Oceanographic Institution.

Restall, S., Jackson, L., Heerten, G. & Hornsey, W., 2002. Case studies showing the growth and developement of geotextile sand containers: an Australian perspective. *Geotextiles and Geomembranes,* Volume 20, pp. 321-342.

Sallenger, A., 2000. Storm Impact Scale for Barrier Islands. *Journal of Coastal Rescearch,* 16(3), pp. 890-895.

Tomasicchop, G. et al., 2011. Large-scale experiments on dune erosion processes. *Journal of Hydraulic Research,* 49(S1), pp. 20-30.

Appendix A

8.1   All Aligned Profile Results
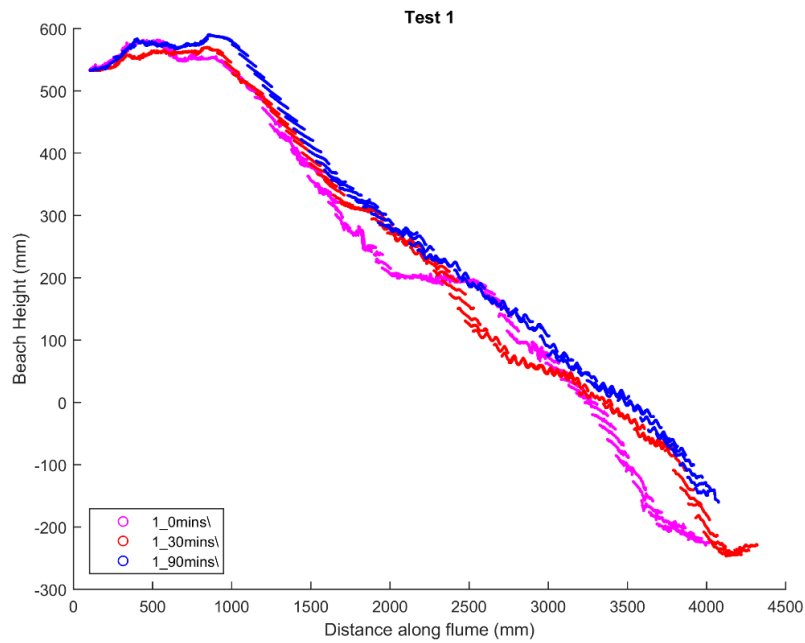
Figure 10: All processed results from Test 1
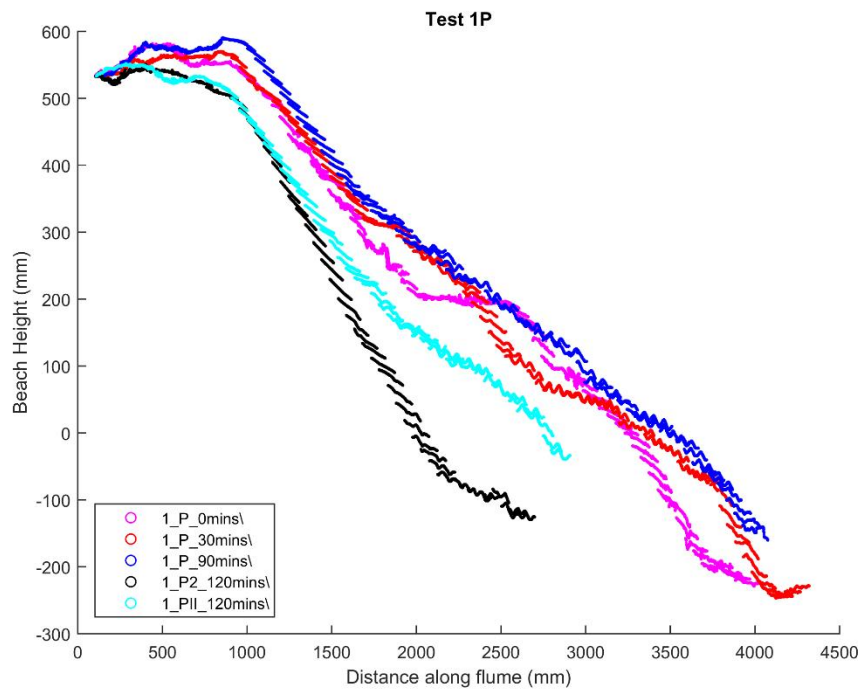
Figure 11: All processed results from Test 1P
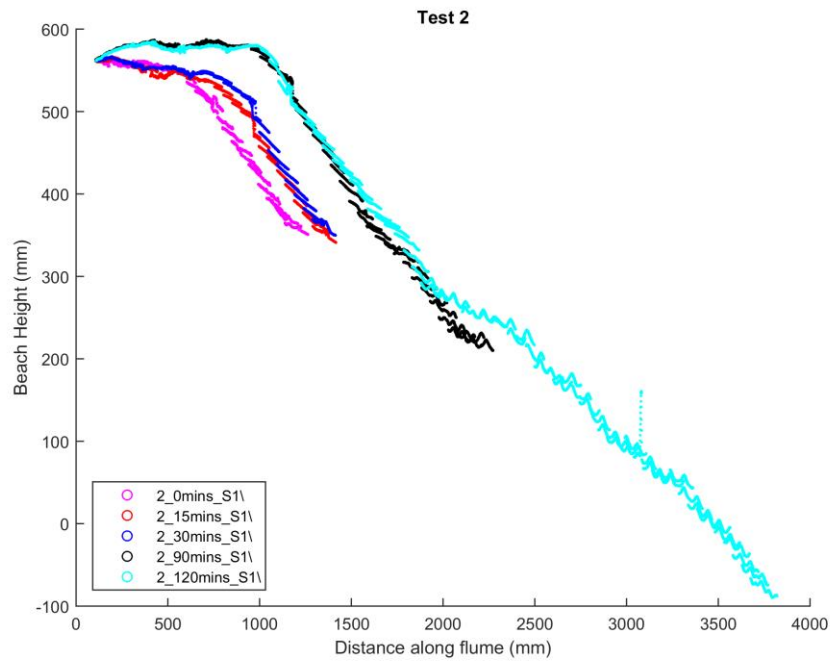
Figure 12: All processed results from Test 2
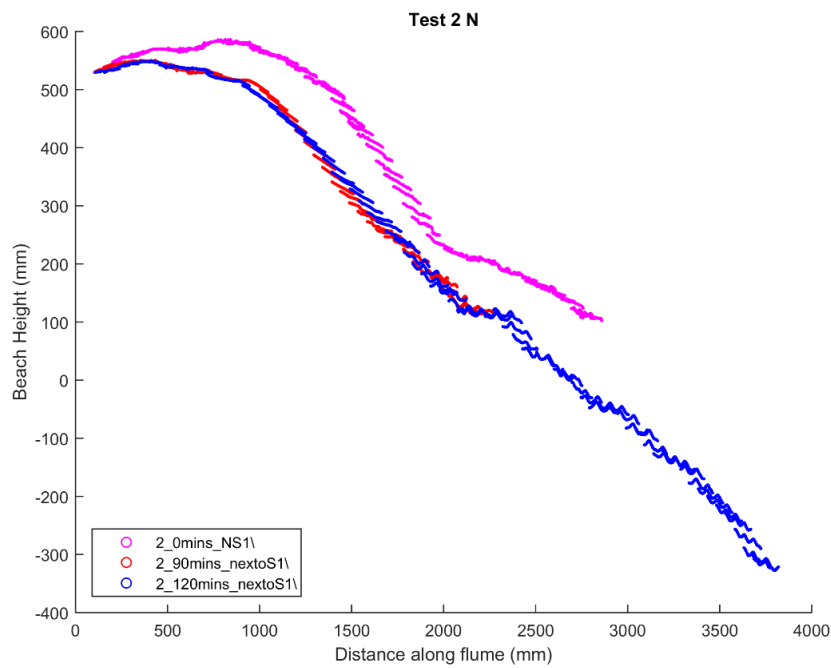
Figure 13: All processed results from Test 2 N
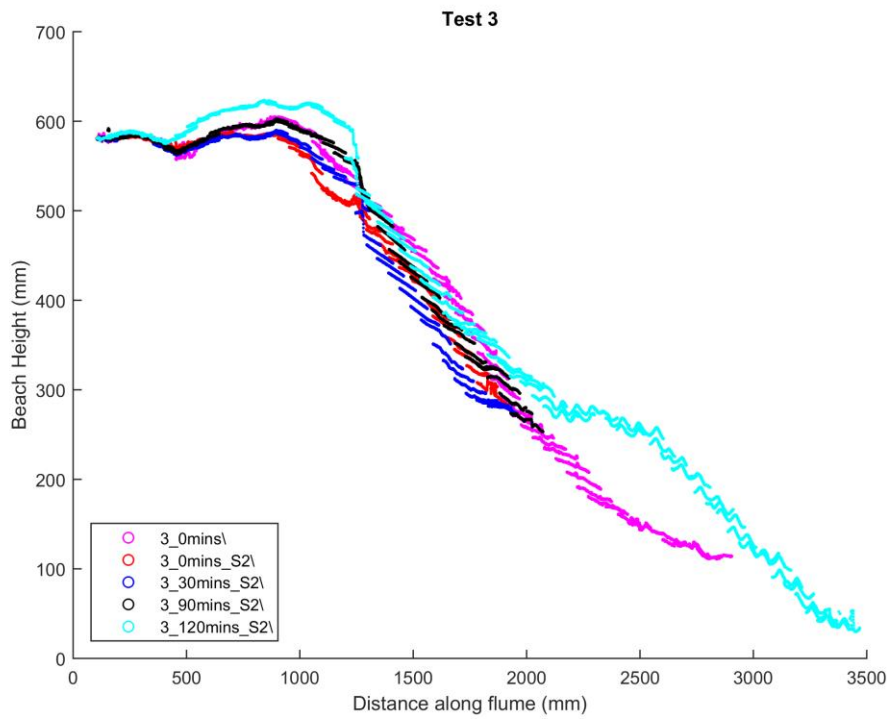
Figure 14: All processed results from Test 3
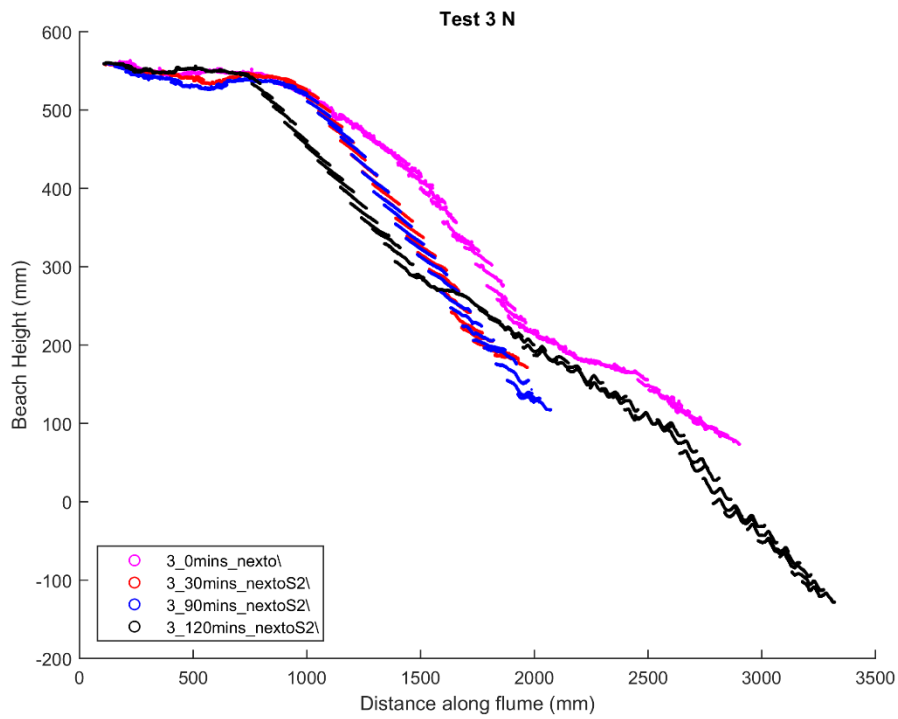
Figure 15: All processed results from Test 3 N
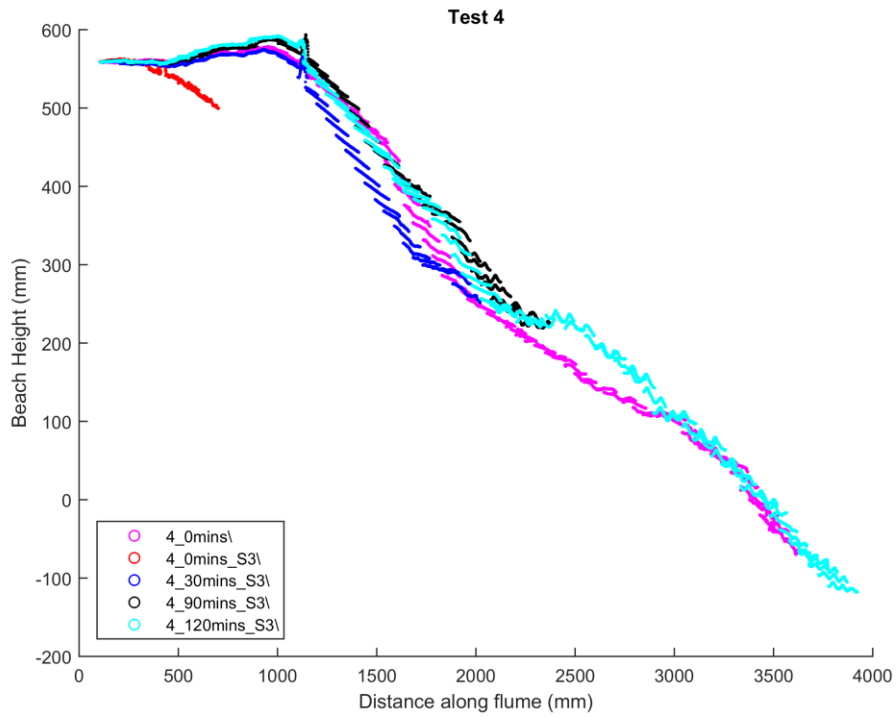
Figure 16: All processed results from Test 4
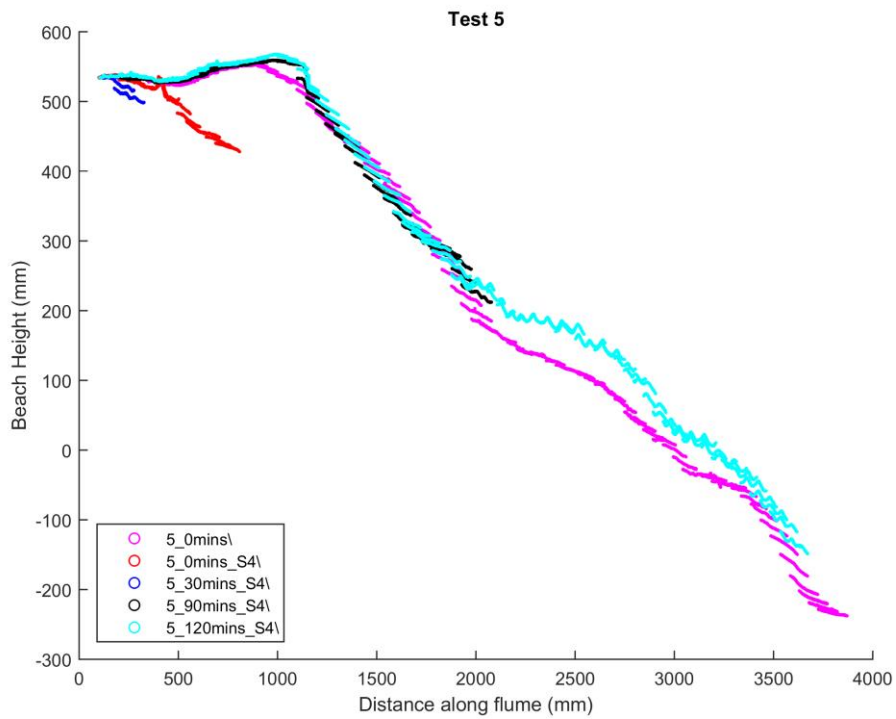
Figure 17: All processed results from Test 5